Wind and Structures, Vol. 11, No. 1 (2008) 1-18
DOI: http://dx.doi.org/10.12989/was.2008.11.1.001

Interference effects in a group of tall buildings closely arranged in an L- or T-shaped pattern

J. G. Zhao† and K. M. Lam‡

Department of Civil Engineering, University of Hong Kong, Pokfulam Road, Hong Kong

(Received December 26, 2006, Accepted January 11, 2008)

Abstract. Interference effects in five square tall buildings arranged in an L- or T-shaped pattern are investigated in the wind tunnel. Mean and fluctuating shear forces, overturning moments and torsional moment are measured on each building with a force balance mounted at its base. Results are obtained at two values of clear separation between adjacent buildings, at half and a quarter building breadth. It is found that strong interference effect exists on all member buildings, resulting in significant modifications of wind loads as compared with the isolated single building case. Sheltering effect is observed on wind loads acting along the direction of an arm of the "L" or "T" on the inner buildings. However, increase in these wind loads from the isolated single building case is found on the most upwind edge building in the arm when wind blows at a slight oblique angle to the arm. The corner formed by two arms of buildings results in some wind catchment effect leading to increased wind pressure on windward building faces. Interesting interference phenomena such as negative drag force are reported. Interference effects on wind load fluctuations, load spectra and dynamic building responses are also studied and discussed.

Keywords: interference effect; wind loads; sheltering; channeling.

1. Introduction

Wind-induced interference effect in closely spaced buildings has been found to result in significant modifications of mean and dynamic wind loads on a building from the isolated single building situation (e.g. Khanduri, *et al*. 1998 for a review). Most studies have been carried out in the wind tunnel in which wind loads are measured on the test building model with the interfering building placed in different relative positions. Interference effects on mean wind pressure and wind forces were studied with rigid building models (Blessman and Riera 1979, Saunders and Melbourne 1979, English 1985). Aeroelastic models and the base-balance technique were later used to assess interference effects on dynamic behaviour of tall buildings (Bailey and Kwok 1985, Taniike 1992, Zhang, *et al*. 1994, Thepmongkorn, *et al*. 2002). A number of interference mechanisms have been reported. Sheltering effect generally leads to reductions in mean wind load on the downstream building but wake buffeting may cause additional fluctuations in wind loads and thus increase the dynamic response of the downstream building. Flow channelling often occurs through the gap

† Graduate Student
‡ Associate Professor, Corresponding Author, E-mail: kmlam@hku.hk

between two closely spaced buildings and this leads to highly negative pressure on the relevant building faces.

In addition to an understanding of the interference mechanisms, recent studies attempted to seek design guidelines for interference effects on wind loads on buildings. Cheng and Lin (2005), and Xie and Gu (2005) commented that the large number of parameters affecting interference effects such as the many possible building arrangements render it impractical to derive simple empirical formulae for interference effect estimation. Data assimilation techniques such as artificial neural network and expert system were recommended as a more sensible approach (English and Fricke 1999, Xie and Gu 2007). A large database of wind loads under interference effects is required for the data assimilation techniques and there are a number of recent wind tunnel measurements towards this effort (Xie and Gu 2004, Huang and Gu 2005, Cheng and Lin 2005). In particular, Xie and Gu (2004) studied interference among three tall buildings and those data of interference effects were recently quantitatively described by a proposed envelope interference factor in Xie and Gu (2007).

Many previous studies report interference between two buildings with a clear building separation between one and a few building width. In metropolitan cities such as Hong Kong, there are many residential developments which comprise a number of similar shaped tall buildings located closely in a group. Building members are often arranged in a row or in an L- or T-shaped pattern and the clear separation between neighbouring buildings is usually less than one building width. In this paper, interference effects on wind loading of five closely-spaced tall buildings arranged in an L- or T-pattern are studied in the wind tunnel from base-balance measurements. The effects of wind incidence angles and spacing separation between neighbouring buildings are investigated. The experimental data will be useful in estimating design wind loads for a group of buildings in close proximity.

2. Wind tunnel experiments

The object of study was a group of tall buildings arranged in an L- or T-shaped pattern. As shown in Fig. 1, five building models were used to achieve the minimum configuration of three member buildings along one arm of the “L” or “T”. All building models were 50cm tall with a square plan form of breadth 10cm. With the target geometric scale at 1:300, they represented typical high-rise residential buildings with height at 150 m and height-to-breadth ratio at 5:1. Two different values of clear building separation were used at $S = 0.25B$ and $0.5B$, B being the building breadth. The experiments were carried out in the boundary layer wind tunnel of the Department of Civil Engineering at the University of Hong Kong. It had a 3.0 m wide and 1.8 m tall working section. With the installation of triangular spires and 8 m long fetch of floor roughness elements, wind characteristics in the tunnel simulated natural wind of the open land terrain type. The mean wind speed profile followed the power law with exponent 0.15 (Fig. 2a). The turbulence intensity varied from a value of about 0.20 near ground to about 0.08 near the roof height (Fig. 2b). These wind characteristics corresponded approximately to those specified for strong winds over the “general” terrain type in the 1983 version of Hong Kong Wind Code (BDD 1983).

Fluctuating wind loads on a building model, including base shear forces F_x, F_y, base overturning moments, M_x, M_y, and torsion M_z, were measured with a six-component force balance (JR3 Inc.) mounted at the model base. From the load signals, mean force and moment coefficients are computed with equations such as:

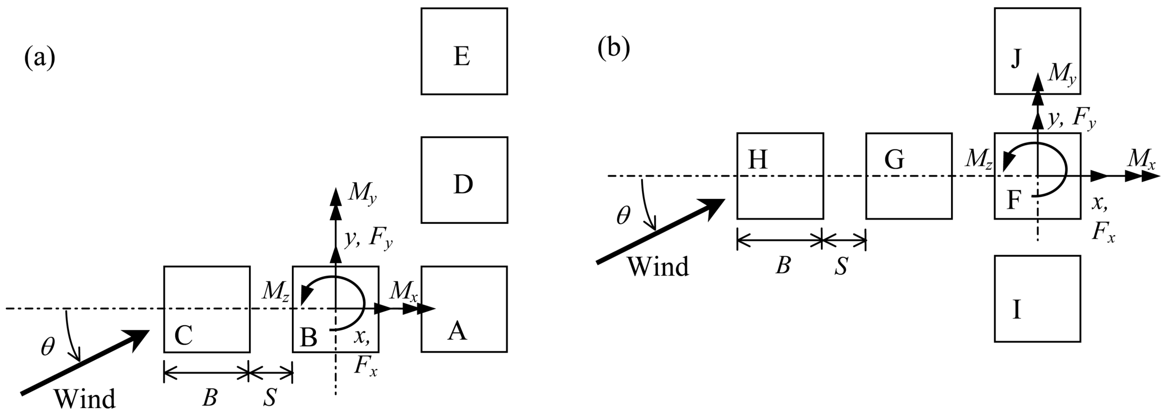

Fig. 1 A group of 5 tall buildings arranged in (a) L-pattern; (b) T-pattern

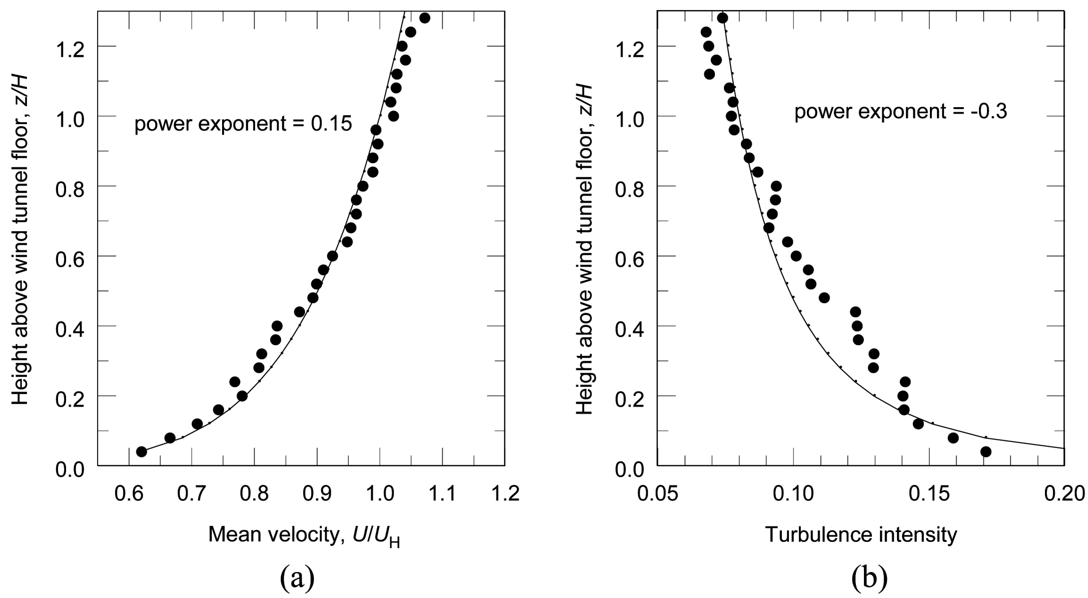

Fig. 2 Wind characteristics in the wind tunnel: (a) mean wind speed profile; (b) turbulence intensity profile

$$
\begin{aligned}
\bar{C}_{F_x} &= \frac{\bar{F}_x}{\frac{1}{2}\rho \bar{U}_H^{\,2} BH} \\
\bar{C}_{M_y} &= \frac{\bar{M}_y}{\frac{1}{2}\rho \bar{U}_H^{\,2} BH^2} \qquad (1) \\
\bar{C}_{M_z} &= \frac{\bar{M}_z}{\frac{1}{2}\rho \bar{U}_H^{\,2} B^2 H}
\end{aligned}
$$

where $\bar{F}_x$ is the mean shear force along the *x*- direction body axis of the building, $\bar{M}_y$ is the mean moment about the y axis of the building and $\overline{M}_z$ is the torsion. The building height is H and $\overline{U}_H$ is unobstructed mean wind speed at the building roof height. Standard deviation values of loading coefficients are computed with equations such as:

$$C'_{F_y} = \frac{\sigma_{F_y}}{\frac{1}{2}\rho \overline{U}_H^2 BH}$$
$$C'_{M_x} = \frac{\sigma_{M_x}}{\frac{1}{2}\rho \overline{U}_H^2 BH^2} \tag{2}$$

where σ_{F_y} and σ_{M_x} are the standard deviations of the base shear force F_y and the base overturning moment M_x, respectively.

Wind load measurements were made at all wind incidence angles to the group of buildings. The definition of wind incidence angle θ is shown in Fig. 1 for the L- and T-patterns of buildings. Making use of the symmetry of the L- or T-pattern and with tests performed at all wind angles between $0^\circ \leq \theta \leq 360^\circ$ at 10° intervals, wind load measurements were made on Buildings A, B and C of one arm of the "L" only. The wind load information on the other two buildings, D and E, could be deduced from the data on Buildings B and C, respectively. For the T-pattern, wind loads were measured on all buildings except Building J whose information could be derived from that on Building I.

3. Results and discussion

3.1. Mean wind loads on buildings of L-pattern

For Buildings A, B and C arranged in one arm of the L-pattern, wind angle variations of the two mean force coefficients, $\overline{C}_{F_x}$ and $\overline{C}_{F_y}$, and mean torsion coefficient, $\overline{C}_{M_z}$, are shown in Fig. 3 for the two building separations. Results for the isolated single building case are also shown for comparison. The overturning moment coefficients, $\overline{C}_{M_x}$ and $\overline{C}_{M_y}$, have the same wind angle variations as the corresponding force coefficients $\overline{C}_{F_y}$ and $-\overline{C}_{F_x}$ and the results are not shown. Since measurements have been made at all wind angles from 0° to 360°, wind load behavior of buildings on the other arm of the L-pattern can be obtained from those of Buildings A, B and C by symmetry. It is evident that the two building separations lead to very similar modifications of wind loads from the isolated single building case, with more significant interference effects at the smaller separation value $S/B = 0.25$.

Between the two shear forces, much larger load reductions from the single isolated building case are observed on $\overline{C}_{F_x}$ which acts along the direction of the arm. This is due to the sheltering effect by upstream building or buildings. The inner Building B experiences the largest reduction in $\overline{C}_{F_x}$ from sheltering effect at nearly all wind directions. The largest magnitude of F_x on Building B is $\overline{C}_{F_x} \approx 0.6$ (occurring at $\theta \approx 120^\circ$) and this represents a 40% reduction from the largest $\overline{C}_{F_x}$ value at 1.0 for the isolated single building case. At wind angles between 0° = 180° and 270°, buildings on the other arm of the "L" provide total shelter to Building B providing almost zero values of C within this quadrant of wind incidence. Building C at the edge of the arm is under strong sheltering effect along the x-direction at wind angles between $\theta = 90^\circ$ and 270° and thus Fig. 3 shows very small values of $\overline{C}_{F_x}$ for Building A at the corner of the "L", sheltering along the x-direction occurs

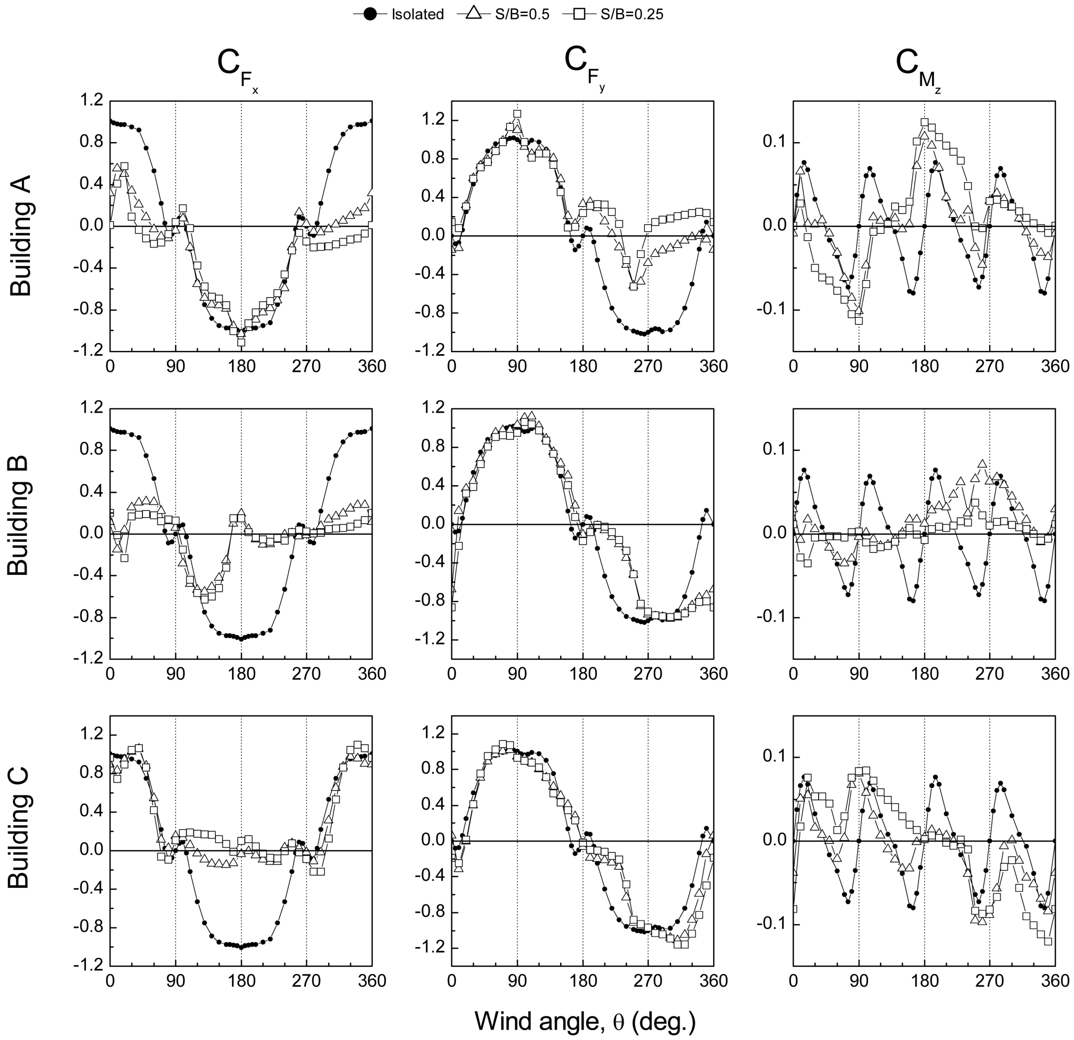

Fig. 3 Mean wind load coefficients: variation with wind angles and effects of building separation (L-pattern)

at the opposite wind incidence angles between $\theta = -90^o$ (that is 270°) and 90°.

A small increase in $\bar{C}_{F_x}$ from the isolated single building case is observed on Building C at $\theta \approx \pm 30^o$. A similar observation has been made for the edge building in a row of tall buildings (Lam and Zhao 2006). At this slightly oblique wind angle, wind hits on the windward *x*-face of Building C in the same way as on a single building, producing similar levels of positive pressure on that face. However, at the leeward side, wind is channeled to flow through the gap between this building and Building B at high speeds (Fig. 1). Highly negative pressure is induced on the leeward *x*-face of Building C. This results in a higher value of F_x than a single building. Similar gap flow is believed to be responsible for the higher on Building A at $\theta = 180^o$. If Building A were alone, wind would separate at its windward corners with diverging separation streamlines and the negative pressure on its leeward face will depend on the distance to the separation streamlines (which entrains air from the face). In the L-pattern, wind flows through the gap between Buildings A and D at high speeds

(Fig. 1). The fast air stream is very close to the leeward face and this results in more negative wind pressure on that face. This leads to high magnitudes of F_x. It is clear in Fig. 3 that the increases in $\overline{C}_{F_x}$ for the two cases become more significant at the narrower building separation. This provides an indirect evidence to the role of the gap flow in the interference mechanism.

Another notable observation on $\overline{C}_{F_x}$ in Fig. 3 is the "negative drag" on Building B at $\theta = 180^o$. The shear force Fx is positive, that is acting in the upwind direction. It is speculated that at this normal wind incidence, wind separates at Building A, and Buildings B and C are inside its wake. Pressure at a point inside the building wake depends on the distance from the separation streamlines extending from Building A. The windward x-face of Building B is nearer to the separation streamlines than its leeward x-face and thus more negative wake pressure is induced on the former face. The result is a small drag force F_x acting upwind.

For the shear force along the y-direction, little interference effects occur on Buildings B and C at wind angles between $\theta = 0^o$ and 180^o. Wind blows freely onto this arm of the "L" and F_y acts perpendicular to the arm (Fig. 1). There is some very slight increase in $\overline{C}_{F_y}$ near $\theta \approx 90^o$ during which high-speed channeled flow through the building gaps causes more negative pressure on the leeward y-faces. Between $\theta = 180^o$ and 270^o, the other arm of the "L" provides some degree of sheltering to Buildings B and C. This reduces the magnitudes of negative pressure on their leeward y-faces and results in small values of $\overline{C}_{F_y}$. In the fourth quadrant, $270^o < \theta < 360^o$, the "L" catches more wind to slow down on windward faces of all buildings. Higher stagnation effects on these faces are believed to cause increased values of $\overline{C}_{F_x}$, especially on Building B.

Building A at the corner of the "L" is shielded by Buildings D and E at wind angles between $180^o < \theta < 360^o$. At $\theta = 180^o$, Building A is under positive F_y at $\overline{C}_{F_y} \approx 0.4$ rather than zero force for an isolated single building. This is because its two y-faces are exposed to different types of flow. On the free side, wind flows around the building the same way as for a single building but on the other side, wind flows through the gap with Building D at highspeed, inducing highly negative pressure on the building faces. In the fourth quadrant of wind incidence, $270^o < \theta < 360^o$, positive values of $\overline{C}_{F_y}$ are found at the narrower building separation of $S/B = 0.25$ instead of negative values for the single building. The cause for this "negative drag" behavior is different from that described above for $\overline{C}_{F_x}$. The windward y-face on Building A is under highly negative pressure due to channeled gap flow while the more exposed leeward y-face is under less negative wake pressure.

Fig. 4 shows that the mean drag coefficient C_D and lift coefficient C_L on buildings in the L-pattern for the wider building separation $S/B = 0.5$. They are computed from the shear force and act in the along-wind and lateral directions. For the isolated single building, C_D is always positive and has a value from 0.9 to 1.2 while C_L changes between −0.3 and 0.3. The phenomenon of negative drag is evidently observed on Building B at $\theta = 10^o$ and 180^o. Building C has almost zero drag at $\theta = 10^o$ and 180^o at this wider S and negative drag occurs when the separation is halved to $S/B = 0.25$ (Fig. 3). Similarly for Building A, the drag has small magnitudes in the fourth quadrant and will turn negative at the narrower building separation. Building C at the end of the arm experiences peak mean drag about $C_D \approx 1.4$ which is about 15% higher than that on an isolated single building. This occurs at $\theta = 330^o$ and is caused by increases in both F_x and F_y as described above. The range of variations of lift force is widened significantly for all three buildings, Buildings A, B and C. On Building A, C_L varies between −0.6 and 0.5. The maximum and minimum lift forces on Building C are about 0.4 and –0.45, respectively. The largest magnitude of peak lift is found on the inner Building B at $C_L \approx -0.7$ occurring at $\theta = 350^o$. This magnitude is more than double the single building value.

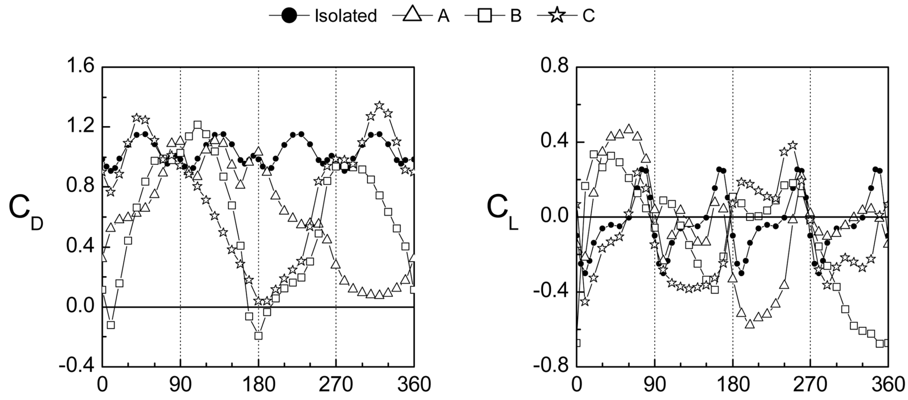

Fig. 4 Variation of mean drag and lift coefficients with wind angles. *S/B* = 0.5 (L-pattern)

Fig. 3 also shows the variation of torsion coefficient $\bar{C}_{M_z}$ with wind angle. Torsion on a square building is caused by the combined effects of asymmetrical pressure distribution on all four building faces. For normal incidence on the isolated single building, separation occurs at the upwind corners and negative pressure on the side face will have large magnitudes near the windward edge and decreasing magnitudes towards the leeward edge. This face produces a significant contribution to torsion. At oblique incidence, positive pressure on the windward face also has an asymmetric distribution and contributes to torsion. It is observed in Fig. 3 that $\bar{C}_{M_z}$ on the inner Building B is much smaller than the isolated building case at wind angles $0^o < \theta < 180^o$. It is believed that channeled gap flow always occurs on its two side faces and their contributions to torsion of opposite signs are balanced out. Between $\theta = 225^o$ to 270^o, torsion on Building B is positive as contrary to the negative torsion on a single isolated building. The negative torsion in the single building case at these wind angles is mainly caused by the asymmetry distribution of positive pressure on the windward building face, that is the right face of Building B in Fig. 1. In the L-pattern, this face is sheltered by the other arm of the “L” and there is thus little contribution to negative torsion. It is expected that flow channeling effect is more intense through the gap on the upper side of Building B than the gap on the lower side. The upper face makes positive contribution to torsion, that is in the counter-clockwise direction.

At most wind angles, torsion on Building C varies within the same range of variation as that of the isolated single building. The exception is around $\theta = 330^o$ when the torsion reaches $\bar{C}_{M_z} < -0.12$, a peak value about 1.5 times the single building value. Similar high values of peak torsion is found on Building A around $\theta = 90^o$ and 180^o. This can be explained by the gap flow on one side face of Building A only. The highly negative pressure on this face with higher levels near the entrance side makes a dominant contribution to torsion.

The peak positive and negative values of mean wind loading coefficients of the Buildings in the L-pattern are summarized and compared with those on an isolated single building in Table 1. The data of all five wind load components are listed for the narrower building separation *S/B* = 0.25 at which the interference effects are generally larger. For the wind loads along the x-direction, Building A at the corner of the “L” and Building C at the end of the arm experience increased peak mean loads which can be 15% higher than the single building values but the increase occurs only over a very narrow range of wind angles (Fig. 3). In many quadrants of wind incidence, wind loads are reduced as a result

Table 1 Peak positive and negative values of mean wind loading coefficients over all wind angles. Building separation at $S/B = 0.25$.

	x-direction loads			y-direction loads			Torsion	
	$\overline{C}_{F_x}$	$\overline{C}_{M_y}$	θ*	$\overline{C}_{F_y}$	$\overline{C}_{M_y}$	θ*	$\overline{C}_{M_z}$	θ*
Single building	±1.01	±0.60	0°, 180°	±1.01	±0.59	90°, 270°	±0.08	90n°±15°
L-Pattern								
A	−1.15	−0.70	180°	1.31	−0.72	90°	−0.12	90°
	−0.60	0.32	20°($\approx 30°$)	−0.53	0.30	180°~360°	0.13	180°
B	−0.65	−0.39	0°~180°	1.10	−0.61	100°	−0.04	20°
	0.21	0.15	0°±90°	−0.99	0.55	180°~360°	0.04	250°
C	1.13	0.73	±20°	1.12	−0.65	70°	−0.12	350°
	−0.23	−0.03	90°~270°	−1.19	0.64	310°	0.09	100°
T-Pattern								
F	−1.02	−0.61	180°	0.52	−0.29	$\approx 110°$	−0.12	0°
	0.38	0.22	−0°	−0.56	0.32	$\approx 240°$	0.09	100°
G	−0.23	−0.15	120°	0.98	−0.55	100°	−0.09	110°
	0.22	0.13	0°±90°	−1.03	0.56	260°	0.10	240°
H	−0.26	−0.06	90°~270°	1.15	−0.65	$\approx 70°$	−0.12	340°
	1.21	0.75	30°	−1.24	0.66	$\approx 310°$	0.09	10°
I	−1.08	−0.64	170°	1.38	−0.79	90°	−0.13	90°
	1.04	0.58	0°~90°	−0.19	0.08	180°~360°	0.11	190°

*Note: This column lists the wind angle θ at which the peak mean load occurs or the range of θ over which the peak mean load occurs.

of sheltering. Building B inside the arm of the "L" is under severe sheltering at nearly all wind angles. All buildings can experience at least 10% increase in mean wind loads in the y-direction at some particular wind incidence angles. For Building A, up to 30% increase can occur.

3.2. Mean wind loads on buildings of T-pattern

Interference effects on mean wind loads on Buildings F, G, H, I in the T-pattern are shown in Fig. 5. Since this pattern of buildings has a plane of symmetry about the line of $\theta = 0°$ or $180°$, Buildings F, G and H have their $\overline{C}_{F_x}(\theta)$ symmetric about $\theta = 180°$ (and $\theta = 0°$) while their $\overline{C}_{F_y}(\theta)$ and $\overline{C}_{M_z}(\theta)$ are anti-symmetry about $\theta = 180°$. For Building H at the long end of the "T", wind angle variations of all three wind load components are almost identical to those of Building C at the end of the "L". This is due to similar wind flow patterns and same interference mechanisms. The only notable difference is that Building H does not experience the sheltering effect on $\overline{C}_{F_x}$ between $\theta = 180°$ and $270°$ which exists on Building C due to the other arm of the "L". For Building G, the behavior of wind loads is very similar to that of the second half part of the load curves for Building B at $180° < \theta < 360°$ in Fig. 3. Around $\theta \approx 240°$, there is a lower degree of shielding offered by Building J in the "T" than the other arm of Buildings D and E in the "L". Hence, both shear forces

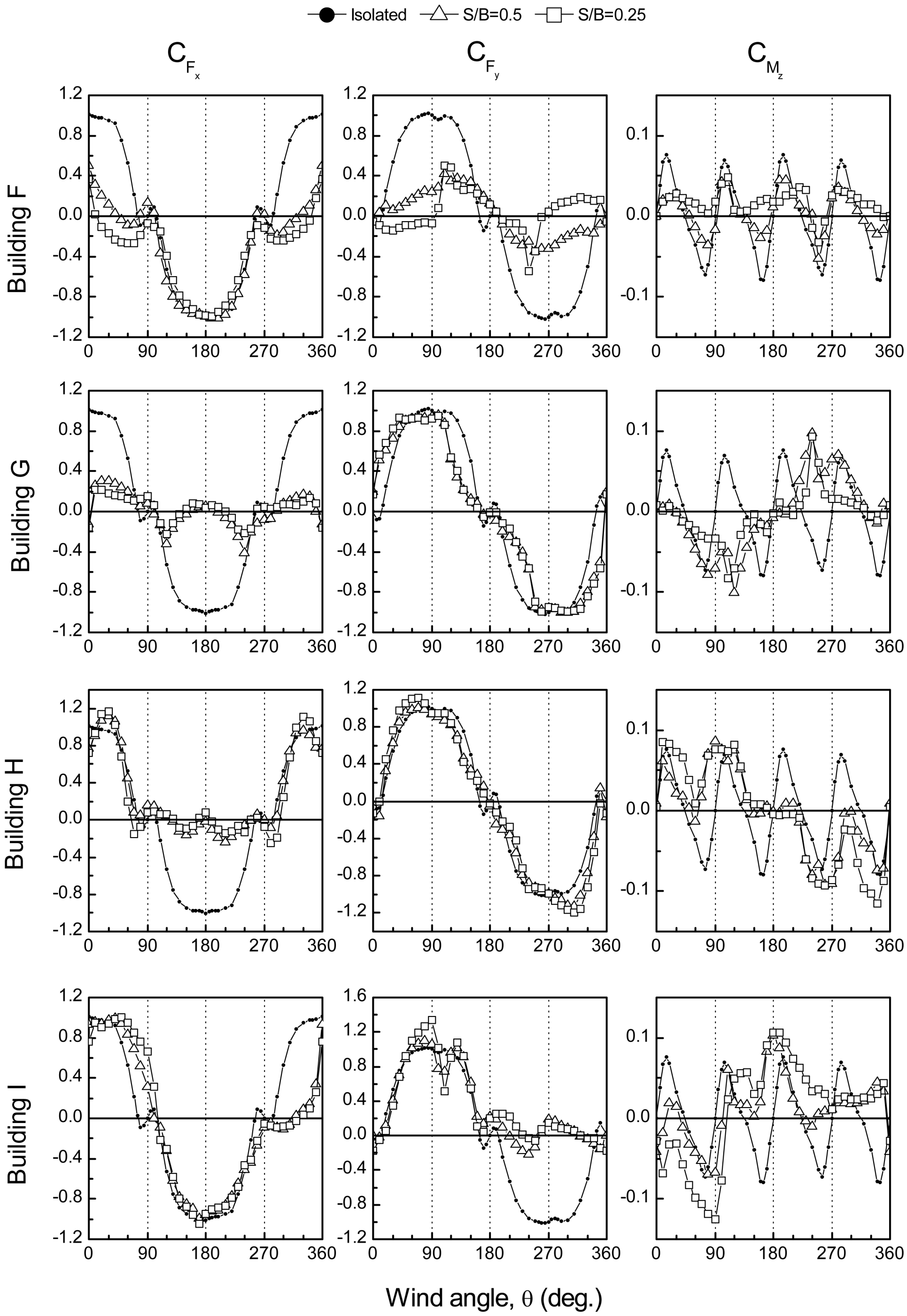

Fig. 5 Mean wind load coefficients: variation with wind angles and effects of building separation (T-pattern)

on Building G are less sheltered than on Building B. Wind load patterns for Building F are similar to those for Building A at 180° < θ < 360°. Some differences are observed near θ = 180° because the interference effects on F_x and F_y found on Building A due to different wind flow behavior around its free and congested faces do not occur on Building F.

For Building I, modification of its C mainly occurs in the fourth quadrant at which its windward x-face is almost totally sheltered by other building members of the "T". This results in near zero values of F_x. Similarly, at $180^o < \theta < 360^o$, its windward y-faces are sheltered resulting in very small values of F_y. At $45^o < \theta < 90^o$, highly negative pressure is expected to occur on its leeward y-face when wind flows through the narrower building gap.

The coefficient becomes larger than the single building value and reaches a peak value at 1.4. The asymmetric distribution of this highly negative pressure on the gap face also produces a peak torsion much larger than the single building peak value.

Table 1 summarized the increase or decrease in the peak positive and negative values of mean wind loading coefficients of the buildings due to building interference as compared to the case of an

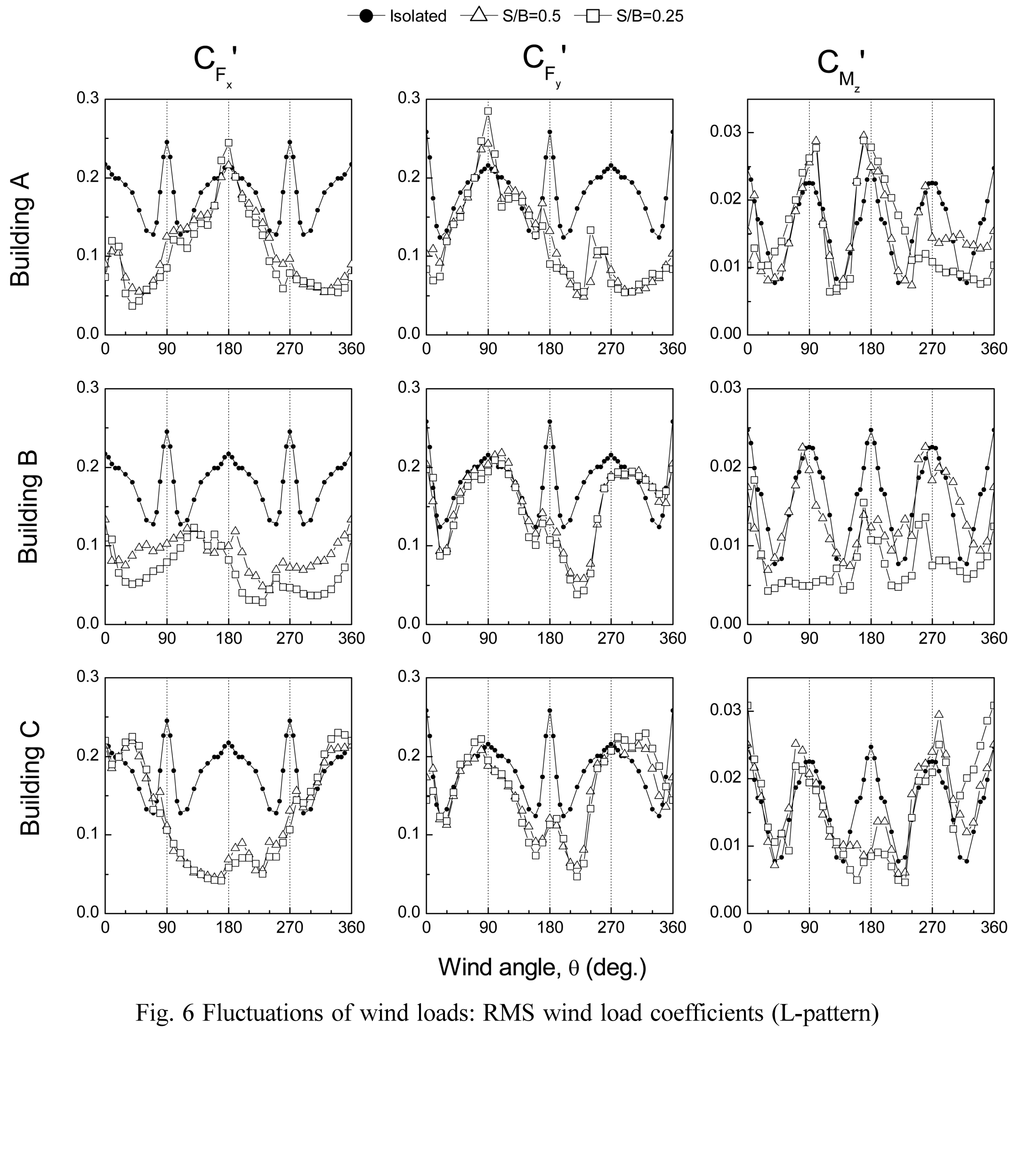

Fig. 6 Fluctuations of wind loads: RMS wind load coefficients (L-pattern)

isolated single building.

3.3. Fluctuation wind loads and load spectra

Fig. 6 shows the coefficients of standard deviation of wind loads on buildings in the L-pattern. These coefficients C'_{F_x}, C'_{F_y} and C'_{M_z} are computed from the time varying wind load signals measured by the base balance. They represent wind load fluctuations acting on the static building models. On an isolated square building, peak values of coefficients occur at normal wind incidences, with turbulence buffeting responsible for load fluctuations in alongwind direction and vortex excitation for the across-wind actions. These mechanisms are evident from the wind moment spectra shown in Fig. 7 At $\theta = 90^o$, for instance, the spectrum of the across-wind moment M_y shows a sharp spectral peak at $nB/\bar{U}_H \approx 0.1$. This is due to vortex shedding from the building and leads to the peak in $C'_{F_x}(\theta)$ in Fig. 6. The along-wind spectrum of M_x is broad-banded without any sharp spectral peaks. This is caused by turbulence buffeting and high values of $C'_{F_y}(\theta)$ occurs over a

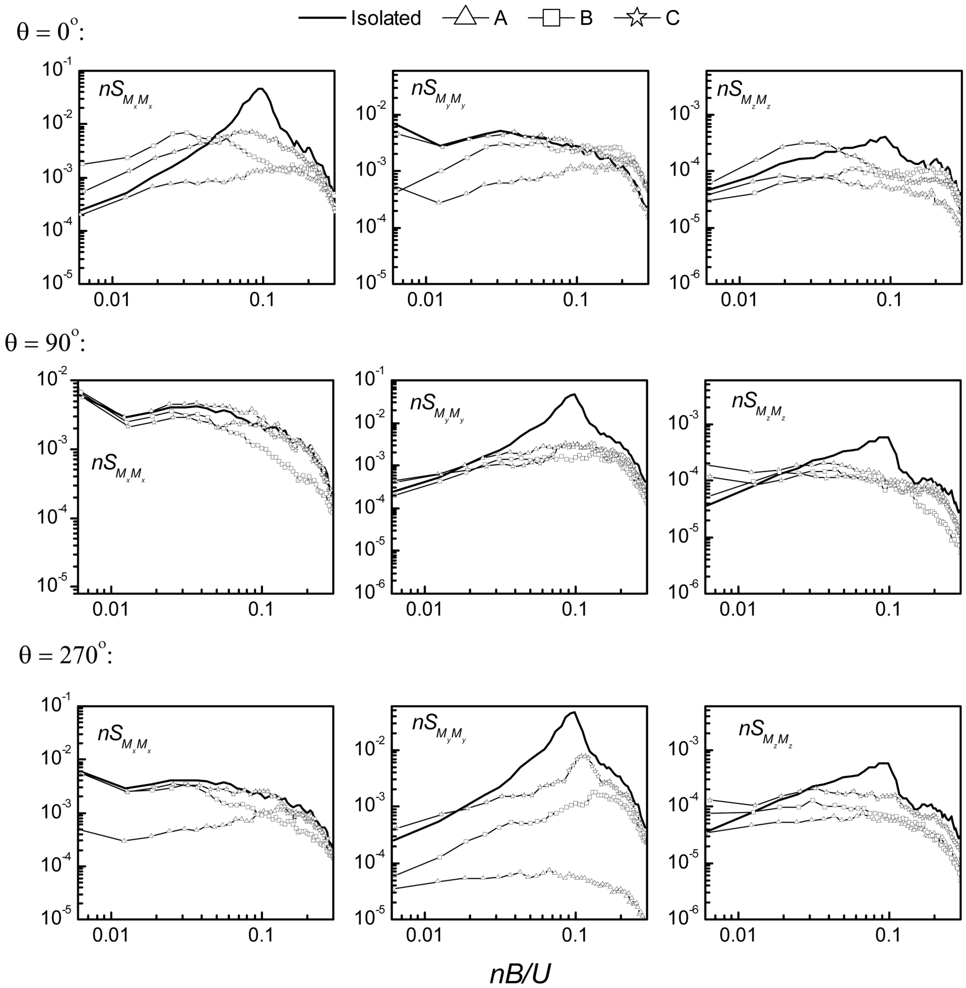

Fig. 7 Wind moment spectra at normal wind incidence. *S/B* = 0.5 (L-pattern)

wider range of wind angles around $\theta = 90^o$.

When buildings are placed in an L-pattern, modifications of standard deviations of wind loads

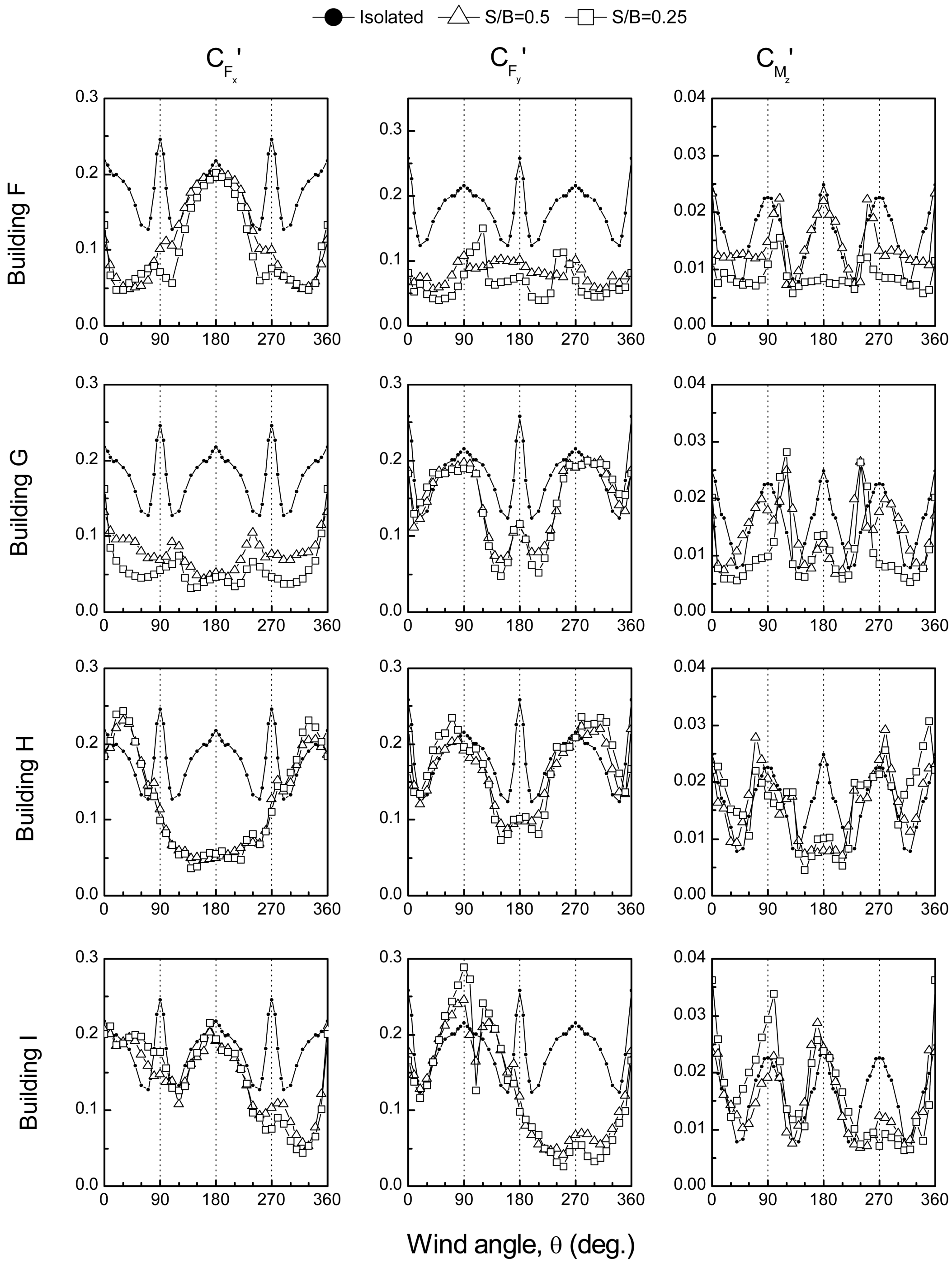

Fig. 8 Fluctuations of wind loads: RMS wind load coefficients (T-pattern)

from the single building case generally follow the same trends as the mean wind loads (Fig. 6 as compared with Fig. 3). At those wind angles when $\overline{C}_{F_x}(\theta)$ is reduced due to the sheltering effect (e.g. on Building C at 90° < θ < 270° in Fig. 3), the standard deviations $C'_{F_x}(\theta)$ are also found to be reduced. Fig. 7 shows that at $\theta = 0^{\circ}$, sheltering effect lowers the broad-banded along-wind moment spectra of M_y on Buildings A and B at most frequencies but there are little changes or even increased spectra power around frequencies $nB/\overline{U}_H \approx 0.2$. Since this frequency is about double the vortex shedding frequency of a square building, this suggests that the sheltered building is under the effect of vortex excitation from the upwind building. However, the sharp vortex shedding peak is not evidently found in the across-wind spectra of M_x at $\theta = 0^{\circ}$ for all buildings in the L-pattern, except a much broader and lower energy peak remaining on the upwind Building C. When wind blows normal to the arm of buildings, around $\theta = 90^{\circ}$ and 270°, turbulence buffeting is not affected or even enhanced by presence of neighboring buildings and thus similar or larger values of C in Fig. 6. For the across-wind force and moment, F_x and M_y, the vortex shedding peak disappears completely. This implies that vortex excitation is greatly reduced on buildings located side-by-side.

Fig. 7 shows that the spectra peak around $nB/\overline{U}_H \approx 0.1$, which occurs in the torsion spectra of an isolated square building, disappears in all buildings in a group. At higher frequencies $nB/\overline{U}_H \approx 0.2$, the spectral levels and shape remain similar. These two observations suggest that modifications in torsion spectra come mainly from increased turbulence in the along-wind actions and lack of vortex-excitation in the across-wind actions.

In Fig. 6, increase in standard deviations of wind loads from the isolated single building case can occur on Building A, B or C at some wind angles. At these wind angles, mean wind loads are also higher than the single building values (Fig. 3) and they are due to channeled flow through building gaps or increased blockage presented by buildings arranged side-byside. Fig. 7 shows that the increase is generally over all spectral frequencies of the broadbanded load spectra.

Fig. 8 shows the coefficients of $C'_{F_x}(\theta)$, $C'_{F_y}(\theta)$ and $C'_{M_z}(\theta)$ on Buildings F, G, H, I in the T-pattern. The same as for the mean wind loads, the behavior of these standard deviation values of wind loads on these buildings follow similar trends as those buildings in the L-pattern at similar relative positions in the group (e.g. Building H and Building C, both on the edge of an arm). For Building I located at the end of the horizontal arm of the "T", the variation of $C'_{F_x}(\theta)$ is similar to Building A of the L-pattern for 180° < θ < 360° and to Building C for 0° < θ < 90°. The variation of $C'_{F_y}(\theta)$ has the same pattern as that on Building A but even higher values are found at 45° < θ < 90°. The moment spectra at normal wind incidences are shown in Fig. 9. When compared to Fig. 7, it is noted that a weaker sharp spectral peak can be found in the across-wind spectra of M_x on Building I at $\theta = 0^{\circ}$, and on Building H at $\theta = 90^{\circ}$ or 270°. It seems that some weak form of vortex shedding can occur from these buildings which are located at the ends of the symmetric T-pattern.

3.4. Dynamic building responses to wind excitation

With the base moment signals measured, wind-induced dynamic deflections of the buildings in the L-pattern or T-pattern are computed with the base-balance technique (Tschanz 1982). With the assumption of linear mode shapes in the sway directions and constant mode shape in the torsional direction, the base moment spectra in Fig. 7 gave the spectra of the generalized wind forces. These spectra are multiplied by the mechanical admittance function of the building to obtain the spectra of building deflections from which the standard deviations of deflections at the building top floor can

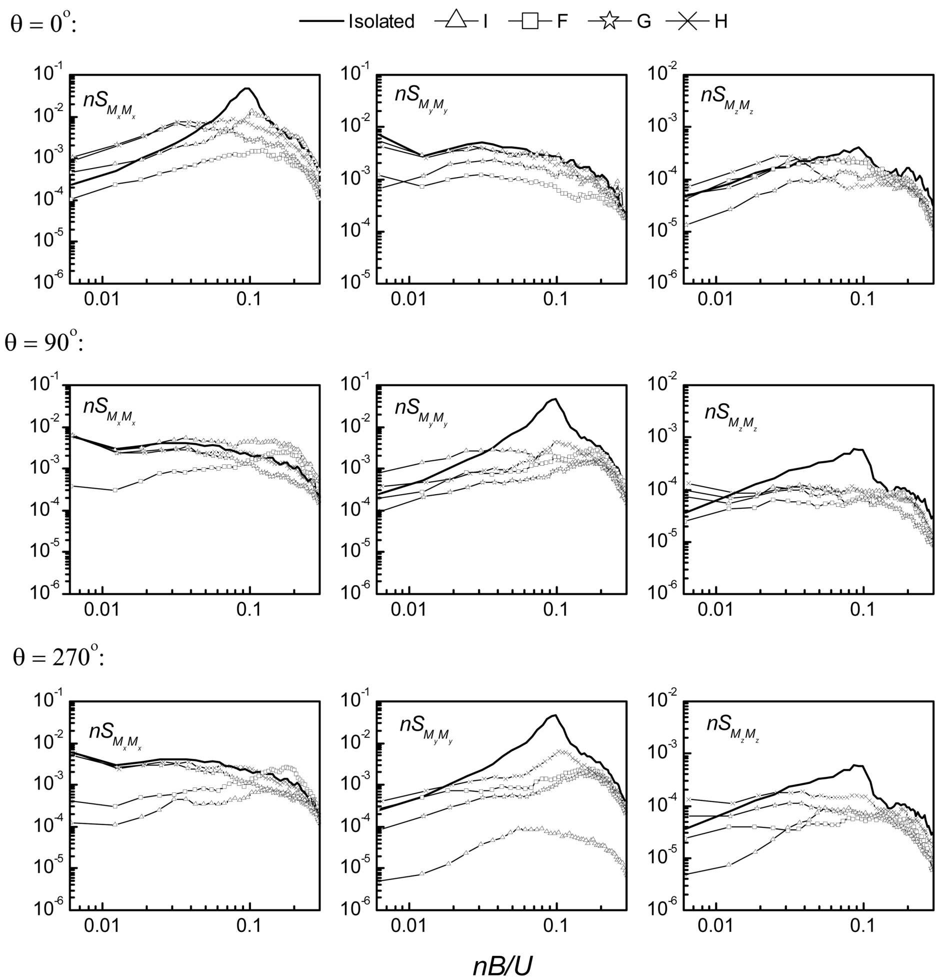

Fig. 9 Wind moment spectra at normal wind incidence. $S/B = 0.5$ (T-pattern)

be found. Dynamic properties of a full-scale 52-storey reinforced concreted residential building of similar height and breadth as the test square building are used for analysis. Same values of fundamental natural frequency and mode shapes are set for the two sway modes: $n_{0,x} = n_{0,y} = 0.238$ Hz and mode shape, $\phi(z) = [0, 0.0015, 0.0040, 0.0070, 0.0101]$ at $z/H = [0, 0.25, 0.5, 0.75, 1]$. The natural frequency for torsion is $n_{0,\varphi} = 0.415$ Hz and a damping ratio at 1% of critical is assumed. The use of this lower value of damping is intended to obtain larger resonant effects which enable clearer observation of the behavior of building responses at different reduced velocities. A damping ratio at 1% is commonly used for assessing wind-induced building accelerations for serviceability purposes.

Figs. 10 and 11 show, for buildings in the L-pattern and T-pattern, respectively, the standard deviations of wind-induced deflections along the sway directions x, y and the torsional direction φ at different reduced velocity at building roof height. Results are shown for the building separation $S/B = 0.5$ only. The data for $S/B = 0.25$ exhibit similar response behavior with reduced velocity and are thus not shown for brevity. For an isolated square building, along-wind responses increases

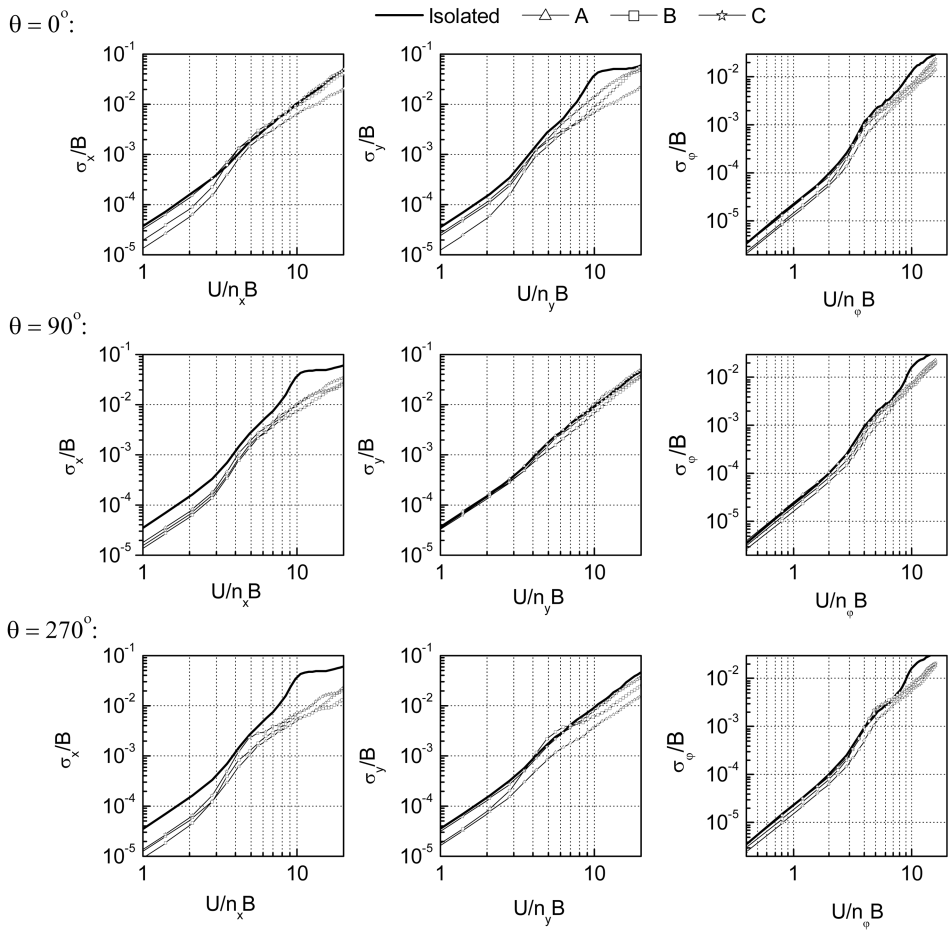

Fig. 10 Wind-induced translational and torsional responses at different reduced wind velocities. *S/B* = 0.5 (L-pattern)

approximately with the square of reduced velocity while across-wind responses show resonant excitation at reduced velocities around 10. This value is the reciprocal of the non-dimensional frequency of the vortex shedding peak in the across-wind moment spectra. Resonant torsion responses are found at reduced velocities around 5 and 10.

For all buildings in the L-pattern, across-wind responses are largely reduced from the single building case with the disappearance of resonant excitation at reduced velocities around 10 (Fig. 10). This is due to the suppression of vortex shedding and vortex excitation for closely spaced buildings. When wind blows along the arm of Buildings A, B and C at $\theta = 0^o$, along-wind responses are reduced for the downwind building but σ_x, of the windward Building C is slightly increased, especially at reduced velocities around 5. At $\theta = 90^o$, when wind blows normal to the arm from the free side of the "L", there is little interference effect on turbulence buffeting and the along-wind responses, σ_y, of Buildings A, B and C are very similar to those of an isolated building. When wind blows from the opposite direction at $\theta = 270^o$, Building A is sheltered and exhibits largely reduced alongwind responses of σ_y. For Building B, the responses become higher than the single building

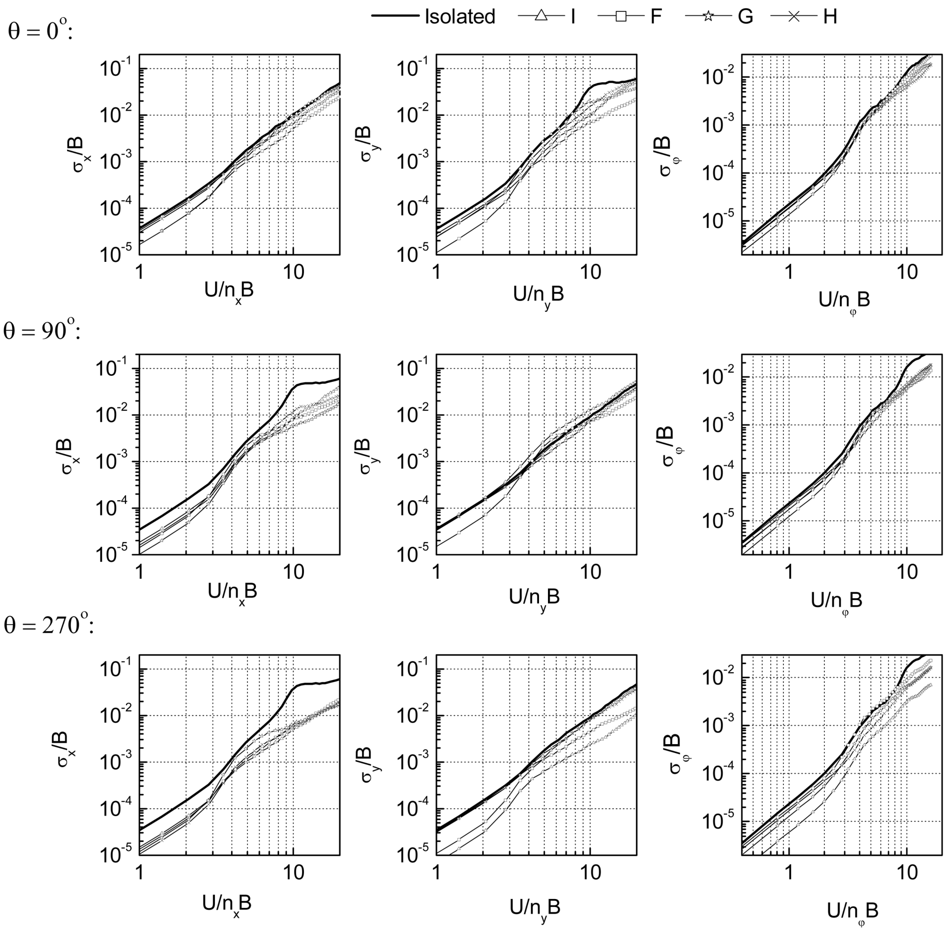

Fig. 11 Wind-induced translational and torsional responses at different reduced wind velocities. *S/B* = 0.5 (T-pattern)

case at reduced velocities around 5.

Similarly, for buildings in the T-pattern, dynamic responses are generally reduced from the single building case (Fig. 11). At $\theta = 0^o$, the moment spectra in Fig. 9 shows some form of vortex shedding from Building I. This explains its resonant across-wind responses of σ_y near reduced velocities 10. Increased *y*-direction wind loads are found on Building I near $\theta = 90^o$ and thus the along-wind responses of σ_y at $\theta = 90^o$ are higher than those of an isolated single building.

4. Conclusions

In this paper, wind tunnel experiments are carried out to investigate interference effects on five tall buildings arranged in an L- or T-shaped pattern. The buildings are square in plan and have a height-to-breadth ratio at 5. The buildings are closely spaced and two values of clear separation between adjacent buildings are tested, one at 0.5*B* and the other at 0.25*B*. Mean and fluctuating wind forces and moments on a building are measured with a base balance for all possible wind incidence angles.

In general, wind loads acting along the direction of an arm of the "L" or "T" are reduced from the isolated building case as a result of sheltering. These wind loads are found to be increased on the upwind building at the end of the arm at a slight oblique wind incidence angle from parallel to the arm. This is caused by wind being channeled to flow fast through the building gap behind the building which produces highly negative pressure on the rear building face. This channeling effect also leads to increase in torsion at some wind angles. When the mean wind loads on a building are increased or reduced due to the interference effect, the fluctuating loads as described by the standard deviations are modified in the same way. The load spectra show that while turbulence buffeting is not very much affected by interference, vortex shedding and the related across-wind excitation are largely suppressed when buildings are closely placed in a group. The computed wind-induced dynamic responses are affected accordingly. In most cases, resonant across-wind responses which occurs on an isolated square building at reduced velocities around 10 are not found on buildings in a group.

Acknowledgement

The investigation is supported by a research grant (HKU7014/02E) awarded by the Research Grants Council of Hong Kong.

References

Bailey, P. A., and Kwok, K. C. S. (1985), "Interference excitation of twin tall buildings", *J. Wind Eng. Ind. Aerodyn.*, **21**, 323-338.

Blessman, J. and Riera, J. D. (1979), "Interaction effects in neighbouring tall buildings", *Proceedings of 5th Int. Conf. Wind Engineering, Fort Collins*, 381-395.

Buildings Development Department, Hong Kong (BDD) (1983), Code of Practice on Wind Effects, Hong Kong.

Cheng, C. M. and Lin, Y. C. (2005), "Interference effects on the design wind loads of tall buildings", *Proceedings of 6th Asia-Pacific. Conf. Wind Engng, Seoul*, 586-598.

English, E. C. (1985), "Shielding factors from wind-tunnel studies of mid-rise and high-rise structures", *Proceedings of 5th US Nat. Conf. Wind Engng, Lubbock*, **4A**, 49-56.

English, E. C. and Fricke, F. R. (1999), "The interference index and its prediction using a neural network analysis of wind-tunnel data", *J. Wind Eng. Ind. Aerodyn.*, 83, 567-575.

Huang, P. and Gu, M. (2005), "Experimental study on wind-induced dynamic interference effects between two tall buildings", *Wind Struct.*, **8**(3), 147-161.

Khanduri, A. C., Stathopoulos, T., and Bedard, C. (1998), "Wind-induced interference effects on buildings . A review of the state-of-art", *Eng. Struct.*, **20**(7), 617-630.

Lam, K. M. and Zhao, J. G. (2006), "Interference effects on wind loads on a row of tall buildings", *Proceedings of 4th Int. Sym. on Comput. Wind Engng., Yokohama*, 817-820.

Saunders, J. W. and Melbourne, W. H. (1979), "Buffeting effects of upwind buildings", *Proceedings of 5th Int. Conf. Wind Engng, Fort Collins*, 593-605.

Taniike, Y. (1992), "Interference mechanism for enhanced wind forces on neighbouring tall buildings", *J. Wind Eng. Ind. Aerodyn.*, **42**, 1073-1083.

Thepmongkorn, S., Wood, G. S. and Kwok, K. C. S. (2002), "Interference effects on windinduced coupled motion of a tall building", *J. Wind Eng. Ind. Aerodyn.*, **90**, 1807-1815.

Tschanz, A. (1982), "Measurement of total dynamic loads using elastic models with high natural frequencies", *Workshop on Wind Tunnel Modeling Criteria and Effects*, N.B.S., Gaithersburg, Mass., 1982.

Xie, Z. N. and Gu, M. (2004), "Mean interference effects among tall buildings", *Eng. Struct.*, 26, 1173-1183.

Xie, Z. N. and Gu, M. (2005), "A correlation-based analysis on wind-induced dynamic interference effects

between two tall buildings", *Wind Struct*., **8**(3), 163-178.
Xie, Z. N. and Gu, M. (2007), "Simplified evaluation of wind-induced interference effects among three tall buildings", *J. Wind Eng. Ind. Aerodyn*., 95, 31-52.
Zhang, W. J., Kwok, K. C. S. and Xu, Y. L. (1994), "Aeroelastic torsional behaviour of tall buildings in wakes", *J. Wind Eng. Ind. Aerodyn*., **51**, 229-248.

CC